Observations of laser driven supercritical radiative shock precursors

S. Bouquet,[1] C. Stehlé ,[2] M. Koenig,[3] J.-P. Chièze,[4] A. Benuzzi-Mounaix,[3] D. Batani,[5] S. Leygnac,[2] X. Fleury,[1] H. Merdji,[6] C. Michaut,[2] F. Thais,[4,6] N. Grandjouan,[3] T. Hall,[7] E. Henry,[3,5] V. Malka,[3] and J.-P. J. Lafon[8]

[1] Département de Physique Théorique et Appliquée (DPTA), CEA-DIF, BP 12, 91680 Bruyères-le-Châtel, France
[2] Laboratoire de l'Univers et de ses THéories (LUTH), Observatoire de Paris, 92195 Meudon, France
[3] Laboratoire pour l'Utilisation des Lasers Intenses (LULI), CNRS - CEA - Université Paris VI - Ecole Polytechnique, 91128 Palaiseau, France
[4] Service d'Astrophysique (SAp), CEA - Saclay, DSM/DAPNIA, 91191 Gif-sur-Yvette cedex, France
[5] Dipartimento di Fisica "G. Occhialini", Università di Milano-Bicocca and INFM, Piazza della Scienza 3, 20126 Milano, Italy
[6] Service Photons Atomes et Molécules (SPAM), CEA - Saclay, DSM/DRECAM, 91191 Gif-sur-Yvette cedex, France
[7] University of Essex, Colchester CO4 3SQ, United Kingdom
[8] Galaxies, Etoiles , Physique et Instrumentation (GEPI), Observatoire de Paris, 92195 Meudon Cedex, France

We present the set-up and the results of a supercritical radiative shock experiment performed with the LULI nanosecond laser facility. Using specific designed targets (small cells with a volume about 1 mm^3) filled with xenon gaz at low pressure (lower than 1 atm), the propagation of a strong shock with a radiative precursor is evidenced. The main measured quantities related to the shock (electronic density and propagation velocity) are shown to be in good agreement with the results obtained from theory and various numerical simulations.

PACS numbers. 62.50.+p, 95.30.Jx, 52.72.+v

Radiative hydrodynamic processes[1,2,3] are very important in several physics areas such as ICF[4] and astrophysics[1,5-7]. Recently, several experiments have been performed to simulate radiative hydrodynamic flows of astrophysical interest like jets or blast waves[8-14] and radiative shocks[15-19]. In most astrophysical environments, such as the envelopes of post-AGB stars, a radiative shock (RS) is essentially characterized by : 1) a hot ionized precursor in the upstream material, heated by radiation coming from the high temperature shocked gas, 2) a shock front followed by a short extension region where relaxation between ions, electrons and photons takes place, and 3) a recombination zone in the downstream flow. In the vicinity of the shock and, provided its velocity is sufficiently high, D_{cr}, the precursor is heated up to a temperature T_{cr} equal to that of the shocked material. Shocks satisfying $D > D_{cr}$ are called "supercritical"[1,3]. The understanding of the properties and structures of these shocks are very sensitive to the treatment of radiation transport and to its coupling with hydrodynamics. Consequently, laboratory experiments[8-19] are very relevant benchmarks for modeling as well as for validating theoretical predictions.

The critical velocity, D_{cr}, above which a radiative shock enters the supercritical regime is approximately given by solving[1,3] the implicit equation $\sigma T_{cr}^4(\rho_1,D_{cr}) = \rho_1 D_{cr} \varepsilon[\rho_1,T_{cr}(\rho_1,D_{cr})]$ where $\varepsilon(\rho,T)$ represents the internal energy (per unit mass) of the fluid ahead the shock and ρ_1 its mass density. This velocity depends, therefore, upon the microscopic properties, $\varepsilon(\rho,T)$, of the material. This steady relation merely assumes that the photon flux emerging from the shock front is completely absorbed to heat (up to the post shock temperature) and to ionize the "dynamically" unperturbed ahead material, at density ρ_1.

In this work, new aspects of the radiative shock are raised compared to the results previously presented in various publications.[8-19] A radiative precursor has been also observed in earlier experiments[9,13,14,16,19] ; however, the authors do not produce flows in a regime similar to the one we achieve. In addition, their goals differ from our about at least two points. First of all, most of the former experiments deal with gas jets containing atomic clusters[9,14,19]. They are rapidly heated by the laser beam and the radiation they emit propagates far away ahead the shock, producing a photo-ionized precursor which is almost not heated since the very low density medium let the radiation escape (in our case, the precursor is heated up to about 15 eV). Second, Taylor-Sedov blast waves, i.e., shock waves created by instantaneous, zero spatial extension explosions, are produced.[9,13,14,16] While it is propagating, the shock weakens rapidly since it is not maintained by additional energy supply. Moreover, the blast wave generates a inner cavity where the mass density decreases with time. In our study, energy is continuously injected (by a piston) in the shock wave and the material is highly compressed behind the shock. This is quite opposite to the situation arising for a blast wave.

In this letter, we present measurements of the velocity and ionization of the precursor of a supercritical shock, and we compare these to simulations. In order to strengthen radiative effects against thermal ones, a low-density material, with high atomic mass, is suitable to achieve high temperature. For that purpose, we choose xenon gas at 0.1 and 0.2 bar (one order of magnitude lower than in Ref. 15). Using a screened hydrogenic type equation of state for xenon, and taking a initial density $\rho_1 = 10^{-3}$ g.cm^{-3}, the critical velocity is found to be as low as $\mathbf{D_{cr} \sim 15\ km.s^{-1}}$, corresponding to the rather small critical temperature $\mathbf{T_{cr} \sim 7\ eV}$. This comfortable low value of the critical velocity is partly due to the high value of the heat capacity of xenon. On the other hand, previous experiments on shock waves, have shown that shock velocities about 50 km/s in a low density medium are achievable with the LULI nanosecond laser facility[20] and it is, therefore, quite suitable to generate supercritical shocks in low density Xe-gas.

However, two important points should be added. First, experiments are performed in small, millimeter size targets and the shock is far from equilibrium, at least regarding its radiative properties. The order of magnitude of the length, L, of a stationary precursor generated by a shock with constant velocity, D, can be derived by equating the diffusion time of radiation (with photon mean free path λ) across the precursor to the time for the material to cover the distance L. One gets $L \sim \lambda c/D$ (c is the velocity of

light), and for the present experiments, we obtain L~1m. The corresponding equilibrium time scale is of the order of L/D, that is, tens of microseconds. From a time-dependent model based on self-similar solutions of the nonlinear heat equation[17], it is found that during the transient phase, the length $l(t)$ of the precursor grows up to its maximum value L according to the law $l(t) = 8.7 \cdot 10^{-7} \cdot (\rho_1[kg.m^{-3}])^{11/36} \cdot (D[m.s^{-1}])^{13/6} \cdot (t[s])^{31/36}$. This length is computed in meter and for D=65km/s and $\rho_1 = 10^{-3}$g.cm^{-3}, we obtain $l \sim 1$m for t=10µs, in agreement with the above result.

Second, according to the Xe shock-adiabat, the compression rate ρ_2/ρ_1 achieved for a shock velocity equal to 65km/s is about 11 in an idealized situation (planar geometry). This result assumes a constant velocity shock, with a fully developed, stationary precursor with constant length L. However, at earlier time the precursor grows up and the value of the radiation flux should be larger than its stationary value. Indeed, in the stationary regime, the energy supplied by the flux is used only to maintain the propagation of the precursor (heating and ionization of the gas) while in the early transient non-stationary phase, the flux should provide energy for both the propagation of the precursor plus its growth, until the steady state be obtained. Consequently, in the transient stage, more energy than in the steady state should be radiated ahead the discontinuity. The temperature of the shocked material is therefore lower than in the final steady and the compression rate can be larger than 11, depending on the magnitude of the emissivity. This interesting property may explain, to some extend, the high compressions achieved by strong shocks propagating in optically thin medium.

According to the former discussion, the experimental diagnostics we used, focus on the time-dependent properties of the radiative precursors produced by strong supercritical shocks. The quantitative design of the whole experiment has been carried out with the radiation hydro-codes MULTI[21] and FCI1[22] (CEA code). A RS is produced with less than a hundred Joules of pulsed laser light. An optimized three layer-pusher drives the shock into the Xe-gas initially at rest in a small quartz cell (about 1mm^3 volume). This pusher is made of a polyethylene ablator slab (2µm), a titanium X-rays screen (3µm) and a polyethylene foam accelerator (25µm). The laser beams focus on the ablator and the foam/Xe interface, that acts as a piston, moves with a maximum velocity about 70 km/s. This high velocity produces the RS together with its radiative precursor in the gas (figure 1).

Experiments have been carried out using three of the six available beams of the LULIÕ Nd-glass laser. The beams were converted at λ=0.53µm, providing a maximum total energy $E_{2\omega} \approx 100$J focused in a spot with diameter 500 µm at FWHM and with a 250µm flat region at the center. Spatially averaged intensities about 4-6$\cdot 10^{13}$ W/cm^2 are achieved, depending upon the laser energy. The laser square pulse has a 120 ps rise-time with a full width at half maximum (FWHM) of 720ps. Each beam is focused with a 500mm lens. Phase zone plates[23] are used in order to remove large-scale spatial modulations of intensity and to get a uniform profile in the spot[24].

The diagnostics we have used in this experiment are shown in Fig.2. The self-emission diagnostic consists in a streak camera recording the emitted light from the rear surface of the target at shock breakout. Two VISARs[25], with different sensitivities (16.63 and 3.39 km/s/fringe) allow us to measure the shock velocity in the foam and/or in the xenon provided the electron density becomes overcritical. Finally, a Mach-Zehnder interferometer is implemented to determine the electron density along the shock propagation. Two streak cameras are used, one looking at the fringes longitudinally (LONG), the other one providing a transverse image at a given position in the gas (TRANS). Assuming a transverse plasma thickness of about 200µm, a electronic density range 10^{18}-10^{20}cm^{-3} in the precursor is inferred from the interferometer.

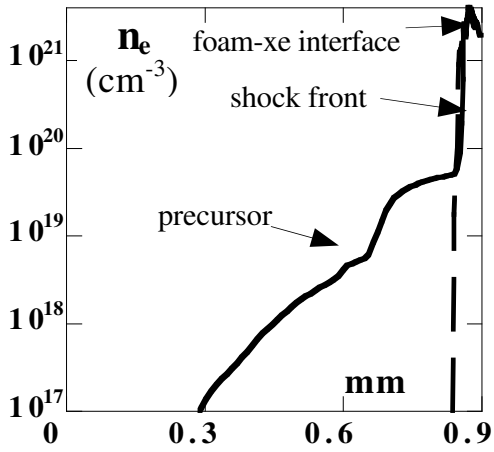

FIGURE 1. Effect of radiation in xenon computed with MULTI hydrocode[21] ($I_L = 6 \cdot 10^{13}$W.cm^{-3}).Non-radiative and radiative cases correspond respectively to the dashed and plain curves.

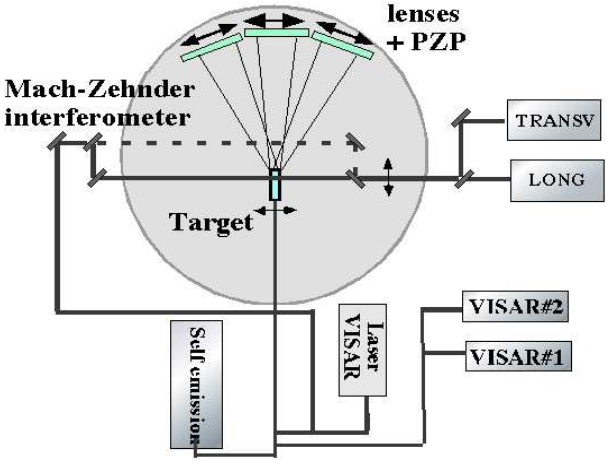

FIGURE 2. Experimental set-up and diagnostics.

With the VISAR, we measure the velocity of the piston (foam/gas interface), which drives the shock in the xenon, provided the gas remains transparent to the probe laser light. As we can see in figure 3, the fringes shift, first, to the left side (velocity jump associated with a small deceleration), then to the right (small acceleration) and finally back to the left.

In this case, the mean measured shock velocity is roughly 67km/s. It is actually four times larger than the critical value D_{cr}. In addition to the fact that numerical simulations show that the shock in Xe is strong enough to create a precursor (Fig.1), the computed velocities are in good agreement with this experimental value. The three

stages described above correspond to the first shock breaking through at the foam/Xe interface, then a second shock arrives (due to a reflection on the pusher interface) and catches the first one and, finally, the piston decelerates slowly (see below).

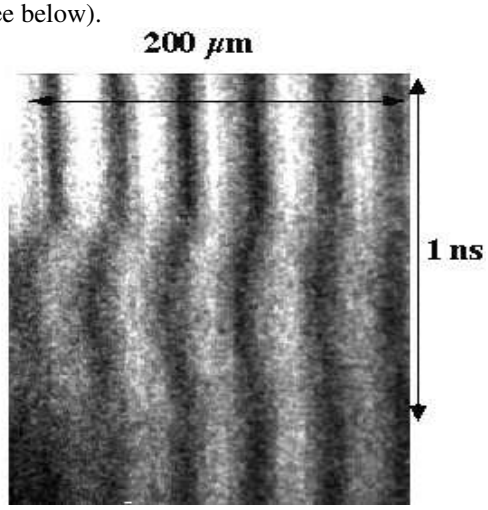

FIGURE 3. VISAR image for a 0.2 bar filled gas cell.

According to the expected shock temperature (about 20˚eV) and the associated ionization-state, the shock front in Xe is overcritical (n_e˚≈˚10^{21}˚cm^{-3}˚)while the precursor is much less than critical (n_e˚†˚10^{20} cm^{-3}˚— Fig.˚1).

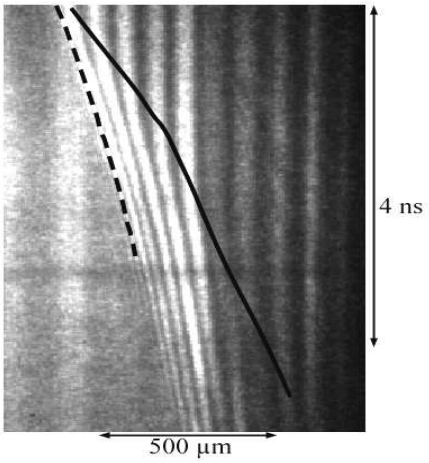

FIGURE 4. Longitudinal interferometry in Xe along the direction of the shock propagation. Dashed and solid lines define the shock and precursor fronts trajectories, respectively.

From the Mach-Zehnder interferometer pattern (Fig.˚4), one may distinguish two different perturbations propagating in the gas. The first one (dashed curve) separates the region where the electronic density is overcritical (to the left of the curve) from the zone in the rear part of the cell where this density is subcritical. It corresponds to the shock front and allows to measure its velocity. During the first 0.4 ns, the value is 68 km/s and decays down to 60 km/s when averaged over the first 3˚ns. This value is very close to the VISAR measurement (67˚km/s). After those 3 ns, it slows down. This is mainly due to the laser pulse duration that is shorter than the time scale evolution of the shock. In addition, on Fig. 4, we also observe clearly fringe shifts, (full line) ahead the shock front, due to a change in the electron density. We associate the region located in between the two lines with the radiative precursor and the full curve represents the position of its front. In accordance with the analytical expression for l(t), the precursor grows roughly linearly with time. Over the first 2˚ns, its velocity (slope of the full line) is close to 130 km/s, which is about twice higher than the piston velocity. Later on, a slow decrease of the precursor velocity occurs due to both the piston deceleration and 2D effects. Those effects have been assessed by the transverse diagnostic (TRANS). Indeed, looking at a given longitudinal position in the cell (≈˚100-200 μm away from the foam interface), we get a picture of the shape of the shock-front in the transverse direction (departure from the plane geometry). The fringe shift is also directly related to the electron density per unit plasma length (≈˚4.5˚10^{21}˚cm^{-3}˚μm^{-1}per fringe). According to the transverse imaging system, a 200˚μm wide plasma is created by the precursor so that one can deduce the variation of n_e(t) — see figure 5.

Numerical simulations clearly show (see below) that the precursor is, in fact, merely a ionized zone with almost no mechanical (or dynamical) effect on the gas. The time-dependent electron density profiles in the precursor can been derived using a reconstuction procedure from the interferograms. The deduced velocities of the ionization wave vary from 70 to 130˚km.s^{-1} for electronic isodensity contours equal to 10^{20}˚cm^{-3} and to 10^{19}˚cm^{-3}, respectively. These results agree rather well with the values of the precursor front and shock velocities obtained in the former paragraph.

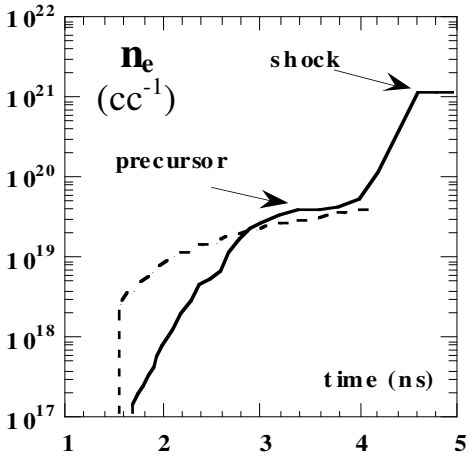

FIGURE 5. Electron density vs time at a given position inside xenon (200˚μm away from the foam interface). Dashed and plain curves come from experiment and simulation results respectively.

The time-dependent formation of the precursor requires a careful numerical calculation of the radiation transport together with a very high spatial resolution. In order to estimate the non-equilibrium effects that govern the early propagation of the precursor, numerical simulations of a supercritical shock, driven by a constant velocity piston, have been performed using the radiative hydrocode ASTROLABE[26]. This fully implicit, moving grid code uses the two moments approximation to compute the radiative transfer and it takes into account non-LTE effects.

Taking a representative piston velocity equal to 65 km/s, the heated material in the precursor remains almost at rest (the gas moves significantly only after the passage of the shock). The gas enters the hydrodynamical shock with a 2 keV kinetic energy per Xe-ion. According to the equation of state of Xe, dissipation of this kinetic energy (through the strong shock) results in a plasma with a mean ionization equal to 15 and a temperature from 32 to 37 eV for densities varying from 10^{-3} g/cm^3 to 10^{-2} g/cm^3.

Figure 6 displays a zoom of the structure of the non-stationary critical shock around the discontinuity, at t = 5 ns. The temperature of both the dense shocked material and the precursor is about 20 eV, which is less than 37 eV. This former value would be only achieved for a steady state, according to the shock adiabat of Xe. The sharp ion-temperature spike at the shock front is a characteristic of supercritical shocks. A fine numerical resolution of the spike by a moving grid method shows that it consists in three distinct regions, each of them exhibiting an increase of the gas compression up to a final value about 55 (depending, actually, on the gas opacity). Shortly after the strong heating of the heavy Xe-ions by the viscous shock (this is the first step of the process and its end is indicated by the cross **X** on the density curve : it corresponds to a compression equal to 4), a first relaxation layer (second step) forms where the ions and electrons temperatures become equal. A second relaxation zone (third step) appears also where the thermal energy of matter is transferred to radiation, on a distance shorter than a photon mean free path, until gas and photons reach the same temperature. This matter-radiation relaxation layer is the source of energy for the shock luminosity (radiative flux) which propagates to heat the gas ahead the shock front and generates the precursor (its actual length is about 500 μm and it cannot be shown on Fig. 6). Unfortunately, the experimental study of the spike properties is beyond the present detector capabilities we used, up to now.

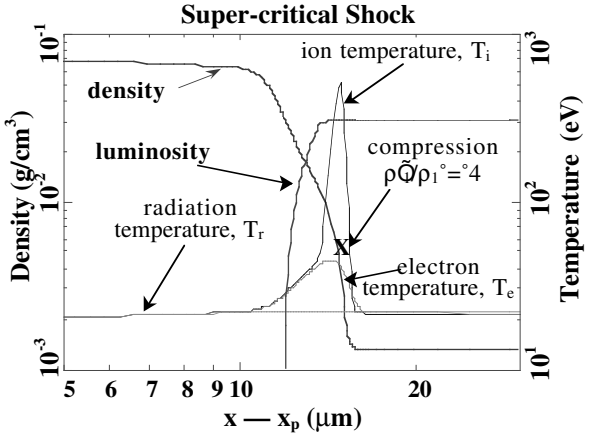

FIGURE 6. Blow-up of the density, temperature and luminosity profiles in the radiative shock at t = 5 ns ($T_i \gg T_e > T_r$). These calculations come from ASTROLABE with the initial condition $\rho_1 = 1.3 \cdot 10^{-3}$ g/cm^3 and $T_1 = 300$ K. The xenon gas is pushed by a 65 km/s piston (x_p represents the piston position) and the density $\rho/\rho = 4\rho_1$ is obtained at the end of the viscous shock.

Experiments have also been simulated with two other dedicated lagrangian radiative 1D hydrocodes, MULTI[21] and FCI1[22]. Both take into account the laser-matter interaction, the actual design of the target and a multigroup radiative transfer, in the diffusion approximation, is used. A detailed comparison of the computed dynamics of the precursor with experiment is somewhat tricky, because it depends upon the value of the electronic density which, in turn, depends on the width of the experimentally probed plasma, estimated with 20% accuracy. However, the similarity between the calculated and the observed structure of the precursor is rather promising (see Fig. 5) since qualitative agreement is obtained. For example, 4 ns after the arrival of the shock wave in xenon and for an electronic density equal to 3.10^{19}/cm^3 (iso-value), the experimental precursor velocity derived from the transverse interferometry is about 100 km/s (see Fig. 4) for a plasma width equal to 200 μm. In the same conditions, the precursor velocity given by the hydrocodes MULTI and FCI1 are respectively equal to 120 km/s and 300 km/s. These velocities have the same order of magnitude but we observe that FCI1 overestimates the value. With a 65 km/s constant piston velocity, ASTROLABE calculates a precursor velocity decreasing with time from 170 to 130 km/s. At t = 4 ns, it is about 150 km/s.

As a conclusion, we have observed, at the LULI facility, the development of a radiative precursor ahead a strong supercritical shock wave, in a xenon gas cell at low pressure. Using various numerous diagnostics, the experimental results we find are in good agreement with numerical simulations. In particular, the measured velocity of the shock front is very close to the value derived from the numerical simulations. The experimental velocity of the precursor remains within the range obtained with the three codes. These discrepancies clearly show that much theoretical and experimental works is required to get a better and reliable modeling of radiative shocks. The quality of our diagnostics will be improved and, in addition, multidimensional effects will be studied, for both hydrodynamics and radiative transfer. In the next future, the upgraded laser facility at LULI will allow to explore the physics of stronger radiative shocks.

Acknowledgements

The authors are very grateful to B. Marchet (CEA/DIF), Ph. Moreau (LULI) and J. Grenier (CEA/Cesta) for their significant contributions to the success of these experiments. They also would like to thank the target designer groups : F. Gex and P. Barroso (GEPI/Observatoire de Paris), L. Polès (CEA/Valduc), and P. Sys, F. David, J. Tidu, P. Di Nicola and B. Cathala (CEA/Cesta). The authors acknowledge the Programme National de Physique Stellaire (CNRS), the Observatoire de Paris and CEA for their financial supports.

References

[1] D. Mihalas and B. W. Mihalas, *Foundations of radiation hydrodynamics* (Oxford University Press, Oxford, 1984)
[2] G. C. Pomraning, *The equations of radiation hydrodynamics* (Pergamon Press, Oxford, 1973)
[3] Y. B. Zeldovich and Y. P. Raizer, *Physics of shock waves and high temperature hydrodynamic phenomena* (Academic Press, New York, 1967)
[4] J. Lindl, Phys. Plasmas **2**, 3933 (1995)
[5] B. Remington, et al., Phys. Plasmas **7**, 1641 (2000)

[6]P.˚Drake, et al., Astrophys. J. **564**, 896 (2002)
[7]S. Bouquet, et al., Astrophys. J. Suppl. **127**, 245 (2000)
[8]D. R. Farley, et al., Phys. Rev. Lett. **83**, 1982 (1999)
[9]T. Ditmire, et al., Astrophys. J. Suppl. **127**, 299 (2000)
[10]A. Frank, et al., Astrophys. J. Lett. **494**, 79 (1998)
[11]S.V. Lebedev, et al., Astrophys. J. **564**, 113 (2002)
[12]A. Ciardi, et al., Laser Part. Beams, **20,** 255 (2002)
[13]J. Grun, et al., Phys. Rev. Lett. **66**, 2738 (1991)
[14]M.˚J. Edwards, et al., Phys. Rev. Lett. **87**, 085004-1 (2001)
[15]J.-C. Bozier, et al., Phys. Rev. Lett. **57**, 1304 (1986)
[16]K.A. Keilty, et al., Astrophys. J. **538**, 645 (2000)
[17]X. Fleury, et al., Laser Part. Beams, **20,** 263 (2002)
[18]P.˚A. Keiter, et al., Phys. Rev. Lett. **89**, 165003-1 (2002)
[19]K. Shigemori, et al., Astrophys. J. Lett. **533**, 159 (2000)
[20]M. Koenig, et al., Phys. Plasmas **6**, 3296 (1999)
[21]R. Ramis, et al., Comp. Phys. Comm. **49**, 475 (1988)
[22]R. Dautray et J.-P. Watteau, *La Fusion Thermonucl aire Inertielle par Laser* (Eyrolles, Paris, 1993)
[23]T. H. Bett, et al., Appl. Opt. **34**, 4025 (1995)
[24]M. Koenig, et al., Phys. Rev. E **50**, R3314 (1994)
[25]P.˚M. Celliers, et al., Applied Phys. Lett. **73**, 1320 (1998)
[26]J.-P. Chi ze, et al., private communication (2002)